Plant Science 370 (2026) 113170

Contents lists available at ScienceDirect

Plant Science

journal homepage: www.elsevier.com/locate/plantsci

Stomatal density and aperture dynamics regulate drought response and yield in tomato

Sanbon Chaka Gosa [1], Bogale Abebe Gebeyo [2], Ravitejas Patil, Ramón Mencia, Menachem Moshelion [*]

The R.H. Smith Institute of Plant Sciences and Genetics in Agriculture, The R.H. Smith Faculty of Agriculture, Food and Environment, The Hebrew University of Jerusalem, Rehovot 76100, Israel

ARTICLE INFO

Keywords:
Functional phenotyping
Crop yield
Dynamic response
Drought stress
Whole-canopy conductance
Tomato introgression lines (ILs)
Stomatal density patterns

ABSTRACT

In crops, key physiological traits such as transpiration, stomatal conductance, and photosynthesis are closely linked to productivity. However, these dynamic traits are often studied under steady-state conditions or modeled with limited data, failing to capture the plant's versatile responses to dynamic field conditions. We hypothesized that natural variation in stomatal morphological traits, specifically, abaxial-to-adaxial distribution and density regulate the temporal physiological response patterns in tomato introgression lines (ILs; crosses between WT, *S. Pennellii*, and M82 lines). We further hypothesized that differences in these response patterns could explain key variations in drought response and yield. To test this, we performed continuous and simultaneous functional phenotyping on IL populations with a well-documented multi-year field yield history. Our results revealed high plasticity in the dynamic water balance regulation of ideotypic ILs (plants with good yield performance under various field conditions). The ideotype lines exhibited higher transpiration and growth rates under well-irrigated conditions than the other lines. Moreover, the ideotype lines exhibited rapid stomatal canopy conductance responses to changing conditions and quick recovery after drought. Anatomically, these lines had high abaxial-to-adaxial stomatal density ratios and stomatal apertures that peaked early in the day, even under water-deficit conditions. Our study demonstrates how a functional phenotyping approach of the whole-plant water-loss measurements can help us understand and identify dynamic, complex, yield-related physiological traits.

1. Introduction

Agricultural crop productivity must increase significantly to meet the food needs of the world's growing population. The challenge of enhancing yields, especially under stressful conditions, while minimizing environmental damage, remains paramount (Tian et al., 2020). Breeding for yield improvement under drought conditions is a very long process (Moshelion and Altman, 2015). Thus, identifying yield-related traits early in growth is a major challenge in pre-breeding programs (Voss-Fels et al., 2019). Stomata play a crucial role in regulating CO_2 uptake and transpiration under water-limited conditions (Endo and Torii, 2019; Harrison et al., 2020). Plants regulate productivity–vulnerability trade-offs by controlling stomatal density, size and aperture (Shahinnia et al., 2016). Measuring canopy conductance and /or stomatal conductance (gs) and transpiration can be another effective screening strategy for plant water-use traits. However, these traits are often studied using steady-state measurements, which fail to capture plant behavior under fluctuating environmental conditions (Matthews et al., 2018), underscoring the importance of measuring the dynamic responses of plants to fluctuating environments (Adachi et al., 2019). Traits like stomatal density, size, aperture, and distribution determine stomatal conductance (gs) and transpiration (Shahinnia et al., 2016; Ohsumi et al., 2007). Moreover, variations in stomatal size and density influence the speed and efficiency of stomatal responses to environmental cues (McAusland et al., 2016) and rapid stomatal responses to light fluctuations were linked with high water use efficiency (WUE) (Battle et al., 2024).

Nevertheless, these traits are challenging to phenotype in a timely manner during an experiment. Recent studies by (Vialet-Chabrand and Lawson, 2019) and (Durand et al., 2019) reported that dynamic models

* Corresponding author.
E-mail address: menachem.moshelion@mail.huji.ac.il (M. Moshelion).
[1] Current address: Carl R. Woese, Institute of Genomic Biology, 1206 W. Gregory Dr., University of Illinois Urbana-Champaign, Urbana, IL 61801, USA
[2] Current address: Department of Horticulture, College of Agriculture and Natural Resources, Dilla University, Dilla, Ethiopia

https://doi.org/10.1016/j.plantsci.2026.113170
Received 13 December 2025; Received in revised form 23 April 2026; Accepted 24 April 2026
Available online 13 May 2026

predict gs more accurately than steady-state models under dynamic environmental conditions. Moreover, continuous whole-canopy conductance (Gsc) measurements in young tomato plants revealed a close relationship between high morning Gsc peak patterns and high yield under field conditions (Gosa et al., 2022a). Yet the measurement of Gsc under dynamic environmental conditions and its environmental interaction is less explored relative to static environmental condition-based measurements. This highlights the need for precise physiological phenotyping for enhanced crop breeding (Ghanem et al., 2015). Hence, whole-plant G×E functional phenotyping platforms are pivotal in addressing such kinds of challenges (Dalal et al., 2020) as these methods measure actual water loss under fluctuating environments. These platforms enable the collection of accurate and continuous data on the entire plant's stomatal behavior in response to its ambient conditions (Jaramillo Roman et al., 2021), which is crucial due to the stomatal dynamic response to both external conditions and the internal biochemical-physiological state. Stomatal ratio between the adaxial and abaxial leaf surfaces directly influences stomatal responses by altering the diffusional pathway for CO_2 uptake and transpiration. Amphistomatous leaves (stomata on both surfaces) generally exhibit higher maximum stomatal conductance and faster gas-exchange kinetics due to reduced boundary layer resistance, but they may also experience greater transpiration demand under high irradiance or low humidity compared to hypostomatous leaves (Xiong and Flexas, 2020; Parkhurst, 1978). Consequently, variation in stomatal ratio modifies the balance between carbon assimilation and water conservation, thereby shaping the sensitivity and magnitude of stomatal responses to environmental drivers such as light, vapor pressure deficit (VPD), and CO_2 concentration (Drake et al., 2013; Muir, 2015).

In C_3 leaves, stomatal density is a primary anatomical determinant of stomatal conductance (g_s), as higher density increases the potential maximum pore area available for diffusion (Franks and Beerling, 2009; Lawson and Vialet-Chabrand, 2019).

In this study, we hypothesize that genotypes with higher early-season cumulative transpiration and faster post-drought recovery accumulate more biomass and achieve higher yields under field water limitation than genotypes with lower water-use efficiency or slower recovery. We further hypothesized that stomatal density ratios, aperture, and physiological response rates to changes in environmental conditions of introgression lines (ILs) will translate into a yield advantage due to water use efficiency under dynamic conditions.

To test the hypothesis, we conducted whole-plant phenotyping in a multi-year field experiment to analyze the yields and plant weights of tomato introgression lines (ILs) that combine S. pennellii genetics with the breeding cultivar M82. We identified 29 ILs exhibiting a range of key traits from high to low yield and resilience and phenotyped their vegetative biomass at the early growth stage and stomatal traits using stomatal imprinting and an automated functional-phenotyping platform. While previous studies have emphasized stomatal traits or steady-state conductance as proxies for drought tolerance and yield, the emerging capability to continuously monitor whole-plant conductance under realistic environmental fluctuations introduces a new dimension of phenotyping. Continuous dynamic phenotyping enables detection of transient peaks, recovery rates, and conductance–environment feedback that cannot be resolved by steady-state approaches. This offers novel mechanistic insight into how stomatal behavior translates into WUE, growth, and ultimately yield, thereby bridging the gap between basic physiology and breeding-relevant performance.

2. Materials and methods

This study combines multi-year field performance data with controlled greenhouse functional phenotyping. First, historic field trials of 29 Solanum pennellii introgression lines (ILs) in the M82 background were used to classify yield and biomass performance under wet and drought irrigation regimes. Based on these classifications, six ILs representing contrasting productivity and resilience profiles, together with M82, were selected for greenhouse testing. In the greenhouse, plants were monitored continuously using the PlantArray gravimetric platform to quantify whole plant transpiration, canopy conductance, drought response and recovery under a feedback-controlled deficit irrigation protocol, and these physiological outputs were linked back to field performance and stomatal traits.

2.1. Field experiment data used for line selection

We analyzed multi-year field yield and biomass data for 29 ILs derived from crosses of *Solanum pennellii* with M82 (*Solanum lycopersicum* cv. M82; Table 1), each containing a unique *Solanum pennellii* chromosome segment (Eshed and Zamir, 1995). In a randomized block design, the field experiments were conducted at the Western Galilee Experimental Station in Akko, Israel, as detailed in (Gur and Zamir, 2004). The experiments were performed at a wide spacing density of 14 plants per 4 m^2. For the dry treatment, only 30 m^3 of water was applied per 1000 m^2 of the field immediately after transplanting. In contrast, the wet treatment received 320 m^3 of water per 1000 m^2 of field area throughout the growing season, in accordance with the area's irrigation protocols. All experiments were conducted using a randomized block design (Fridman et al., 2000). Multi-year field data guided the selection of high- and low-to-medium-performing introgression lines for greenhouse plant-array tests to characterize physiological performance. These irrigation values derive from the original historic field trials used for line classification and were not part of the present greenhouse experiment. Data on weather conditions, including radiation, temperature, and humidity, from the nearest meteorological station to the experimental site indicate typical summer weather for the area (Supplementary Tables 1 and 2).

2.2. Experimental setup for functional phenotyping

Selected ILs based on their multiple-year (2000–2004) fruit and biomass yield performance from low to high yield as compared to the M82 tomato plants were grown in a greenhouse at the Israeli Center of Research Excellence (iCORE) (https://researchinfrastructure.inwise.net/iCORE); The Hebrew University of Jerusalem, at Rehovot campus during September 2019. The protocols and methods of the PlantArray system have been detailed in previous studies (Dalal et al., 2020) (Halperin et al., 2017). Here, we provide a brief description along with specific protocols for the current experiment. The iCORE polycarbonate greenhouse features cooling pads activated when the temperature reaches 32 °C. A weather station in the greenhouse near the plants continuously monitored weather conditions. The continuous photosynthetic photon flux density (PPFD) and vapor pressure deficit (VPD) measured during the experimental period are presented in Fig. 3A. Before the start of the experiment, all load-cell units were calibrated for accuracy and drift level under constant load weights (1 kg and 5 kg) using the PlantArray auto-calibration application.

The setup consisted of highly sensitive, temperature-compensated load cells used as weighing lysimeters. Each measuring unit was mounted with a 4 L pot containing a single plant and connected to its controller, which collected data and controlled irrigation. Each pot was placed into the plastic container through a hole in its cover and an 'O'-ring to prevent water evaporation from the bottom of its drainage holes. The containers had orifices at identical heights on their side walls to enable similar water levels after drainage of excess water following irrigation. Evaporation from the pot surface was prevented by a soil cover with a circular cutout at its center, through which the plant would grow.

Tomato seeds were germinated in cavity trays in the greenhouse. Five-week-old seedlings of the selected ILs and M82 tomato plants were transplanted into 4 L pots filled with quartz sand 20/30 (the upper and lower size of the mesh screen through which the sand was passed; 20 =

Table 1
Phenotypic classification of tomato introgression lines based on total yield and plant weight under well-irrigated and dry field conditions (as presented in Fig. 2). Relative to M82, lines were classified into three groups based on their fruit weights: high-yielders (HY, >20%), low-yielders (LY, 20%) and medium-yielders (MY, similar). Similarly, lines were classified as high biomass (HB), medium biomass (MB) and small biomass (SB), relative to M82. Lines with all "highs" were considered ideotypic. The drought stress-response phenotype was classified based on terminology suggested by Moshelion (2020). Specifically, under drought conditions a line with a fruit weight that was 20% higher fruit than that of M82 was classified as having a high tolerance (HT), a line with a fruit weight that was 20% lower than that of M82 was classified as having a low tolerance and lines with fruit weights similar to that of M82 were classified as having moderate tolerance (MT). Plants that maintained or increased their biomass under stress were categorized as having a high resilience (HR). Plants that maintained or reached medium levels of shoot biomass were classified as medium resilience (MR). Small plants that maintained their size or larger plants that lost biomass under stress were classified as having low resilience (LR); the former phenotype was also referred to as a survival phenotype. We identified 20 classification groups; seven of which (marked with *) were selected for further physiological characterization using the functional telemetric platform. All these lines exhibited consistent behavior across the years of study data.

Line	ID Number	Fruit yield	Shoot weight	Fruit yield	Shoot weight	Group classification	Abbreviation	Classification Number	
M82	30	**CONTROL**	**CONTROL**	**CONTROL**	**CONTROL**	Control			*
IL12–1–1	4	**HIGH**	**HIGH**	**HIGH**	**HIGH**	High yielder High biomass High tolerance High resilience - IDEOTYPE	HyHbHtHr	1	
IL5–2	16	**HIGH**	**HIGH**	**HIGH**	**HIGH**	High yielder High biomass High tolerance High resilience - IDEOTYPE	HyHbHtHr	1	*
IL6–4	26	**HIGH**	**HIGH**	**HIGH**	**HIGH**	High yielder High biomass High tolerance High resilience - IDEOTYPE	HyHbHtHr	1	
IL7–4–1	22	**HIGH**	**HIGH**	**HIGH**	**HIGH**	High yielder High biomass High tolerance High resilience - IDEOTYPE	HyHbHtHr	1	
IL2–4	8	**HIGH**	**HIGH**	**MEDIUM**	**HIGH**	High yielder High biomass Medium tolerance High resilience	HyHbMtHr	2	
IL2–6	9	**HIGH**	**HIGH**	**LOW**	**HIGH**	High yielder High biomass Low tolerance High resilience	HyHbLtHr	3	*
IL11–4	3	**HIGH**	**MEDIUM**	**MEDIUM**	**MEDIUM**	High yielder Medium biomass Medium tolerance Medium resilience	HyMbMtMr	4	*
IL6–3	20	**MEDIUM**	**HIGH**	**LOW**	**HIGH**	Medium yielder High biomass Low tolerance High resilience	MyHbLtHr	5	
IL9–3	29	**MEDIUM**	**HIGH**	**LOW**	**HIGH**	Medium yielder High biomass Low tolerance High resilience	MyHbLtHr	5	
IL9–1	26	**MEDIUM**	**HIGH**	**LOW**	**MEDIUM**	Medium yielder High biomass Low tolerance Medium resilience	MyHbLtMr	6	
IL9–2–6	28	**MEDIUM**	**HIGH**	**MEDIUM**	**HIGH**	Medium yielder High biomass Medium tolerance High resilience	MyHbMtHr	7	
IL2–6–5	10	**MEDIUM**	**MEDIUM**	**HIGH**	**HIGH**	Medium yielder Medium biomass High tolerance High resilience	MyMbHtHr	8	
IL5–3	17	**MEDIUM**	**MEDIUM**	**MEDIUM**	**HIGH**	Medium yielder Medium biomass Medium tolerance High resilience	MyMbMtHr	9	
IL9–1–3	27	**MEDIUM**	**MEDIUM**	**MEDIUM**	**LOW**	Medium yielder Medium biomass Medium tolerance Low resilience	MyMbMtLr	10	
IL10–2	2	**MEDIUM**	**MEDIUM**	**MEDIUM**	**MEDIUM**	Medium yielder Medium biomass Medium tolerance Medium resilience	MyMbMtMr	11	
IL5–5	18	**MEDIUM**	**SMALL**	**HIGH**	**HIGH**	Medium yielder Small biomass High tolerance High resilience	MySbHtHr	12	
IL2–1–1	7	**MEDIUM**	**SMALL**	**MEDIUM**	**LOW**	Medium yielder Small biomass Medium tolerance Low resilience	MySbMtLr	13	
IL12–2	5	**MEDIUM**	**SMALL**	**MEDIUM**	**MEDIUM**	Medium yielder Small biomass Medium tolerance Medium resilience	MySbMtMr	14	
IL12–3–1	6	**MEDIUM**	**SMALL**	**MEDIUM**	**MEDIUM**	Medium yielder Small biomass Medium tolerance Medium resilience	MySbMtMr	14	
IL10–1	1	**LOW**	**HIGH**	**LOW**	**HIGH**	Low yielder High biomass Low tolerance High resilience	LyHbLtHr	15	*
IL3–3	11	**LOW**	**HIGH**	**LOW**	**HIGH**	Low yielder High biomass Low tolerance High resilience	LyHbLtHr	15	
IL3–4	12	**LOW**	**HIGH**	**LOW**	**HIGH**	Low yielder High biomass Low tolerance High resilience	LyHbLtHr	15	
IL6–2	19	**LOW**	**MEDIUM**	**LOW**	**LOW**	Low yielder Medium biomass Low tolerance Low resilience	LyMbLtLr	16	
IL4–1	13	**LOW**	**MEDIUM**	**MEDIUM**	**MEDIUM**	Low yielder Medium biomass Medium tolerance Medium resilience	LyMbMtMr	17	
IL4–1–1	14	**LOW**	**SMALL**	**MEDIUM**	**MEDIUM**	Low yielder Small biomass Medium tolerance Medium resilience	LySbMtMr	18	
IL8–1	23	**LOW**	**SMALL**	**LOW**	**MEDIUM**	Low yielder Small biomass Low tolerance Medium resilience	LySbLtMr	19	*
IL8–1–3	25	**LOW**	**SMALL**	**LOW**	**LOW**	Low yielder Small biomass Low tolerance Low resilience - SURVIVAL	LySbLtLr	20	*
IL4–3–2	15	**LOW**	**SMALL**	**LOW**	**LOW**	Low yielder Small biomass Low tolerance Low resilience - SURVIVAL	LySbLtLr	20	
IL8–1–1	24	**LOW**	**SMALL**	**LOW**	**LOW**	Low yielder Small biomass Low tolerance Low resilience - SURVIVAL	LySbLtLr	20	

20 squares across one linear inch of screen), resulting in a sand particle size of between 0.595 and 0.841 mm (Negev Industrial Minerals Ltd., Israel).

Fertilizer (poly feed 17:10:27, Haifa Chemicals, Haifa, Israel) was supplied to the plants through the irrigation system known as fertigation. Each pot was fertigated with four drippers inserted into the upper portion of the sand to ensure that the medium was uniformly wet with each irrigation event. Fertigation was applied during the night in multiple pulses. The fertigation in the control treatment consisted of four irrigation pulses, each lasting 15 min, applied every 2 h to ensure adequate leaching and achieve full pot water capacity.

2.3. Enhancing signal-to-noise in greenhouse phenotyping

The phenotyping system employed several strategies to enhance the signal-to-noise ratio, thereby reducing potential artifacts in the noisy greenhouse environment. These strategies include the use of high-accuracy load cell transducers, achieving a precision of ±0.167 g per kg of load on each cell. These transducers are also temperature-compensated to minimize drift caused by ambient temperature fluctuations effectively. Furthermore, each load cell is connected via a short cable (45 cm) to its analog-to-digital (A/D) controller, significantly reducing analog electrical interference and noise (typically associated with long cables connected to a central data logger). Thermal insulation and sealed covers are applied separately to each load cell to prevent overheating due to direct solar radiation. Vibration-induced noise is mitigated by placing compressed foam cushions and mass under each load cell. Measures to counteract the "pot effect" (Gosa et al., 2019), such as double-pot arrangements that isolate the soil and roots from direct solar radiation-induced heat, periodic flushing to prevent salinity buildup from frequent fertigation, and a split-dripper system to avoid localized soil compaction from uneven water distribution, ensuring the reliability and consistency of the physiological data collected during the experiment.

2.4. Drought treatment

To standardize drought stress across genotypes with different transpiration rates, we used the PlantArray system to apply feedback-controlled deficit irrigation. Each plant's daily irrigation was set to 80% of its transpiration from the previous day, ensuring that fast-transpiring plants received proportionally more water than slow-transpiring plants. This imposed a similar dehydration trajectory across plants while preserving genotype-specific differences in water use and dynamics. This protocol was applied throughout the drought-imposition phase until re-irrigation (Fig. 3C). To avoid confounding drought effects with nutrient limitation, plants continued to receive the same nutrient solution via fertigation during the drought-imposition phase, but in the reduced irrigation volumes determined by the feedback-controlled deficit protocol.

Here, θcrit was defined as the soil volumetric water content (VWC) at which transpiration began to decline from the well-irrigated plateau for an individual plant, and it was used as a standardized reference point for comparing genotypic drought responses. This approach prevented a rapid decrease in soil water content, creating a uniform drought scenario throughout the treatment period (see Fig. 3B in (Dalal et al., 2019). Using this approach, even the rapid water-loss lines (e.g., IL11–4) showed no significant differences between treatments across soil moisture levels. Such precise treatment-control mechanisms are necessary to maintain consistent and replicable conditions across all experimental units, as emphasized by the JXB guidelines for drought experiments (Moshelion et al., 2024). These guidelines advocate standardizing experimental conditions to minimize variability and enhance reproducibility, thereby ensuring that observed differences in plant responses are attributable to genetic variation rather than environmental variation (Franks and Beerling, 2009).

2.5. Selection of introgression lines for the physiological experiment

Following the classification and the terminology proposed by (Moshelion, 2020), plant drought-response behavior was defined as follows: Plant resilience (recovery from stress) was determined by the plant's biomass relative to M82, under similar drought conditions, and plant tolerance was measured by its total yield (TY) under identical drought conditions. In this context, resilience refers to the plant's capacity to recover biomass identical to that of M82 after re-irrigation. At the same time, tolerance is defined as the plant's ability to maintain or increase yield under stress. Thus, under comparable drought stress, a line displaying higher biomass and higher yield would be classified as having a high-resilience (HR) and high-tolerance (HT) phenotype (HrHt). In contrast, a line with lower biomass and yield under drought conditions would be classified as having a low-resilience (LR) and low-tolerance (LT) phenotype (LrLt). If a line's biomass under stress was $>$ 20% of the control, but its yield was lower than M82, it was defined as high-resilience–low-tolerance (HrLt; Table 1). This categorization yielded 20 groups, ranging from ideotypic to survival phenotypes.

2.6. Measurement of quantitative physiological traits

Plant water relations, kinetics, and physiological traits were determined for all plants by continuously and simultaneously monitoring soil-plant-atmospheric conditions, as shown in Fig. 1. Whole-plant physiological traits were measured using the PlantArray 3.0 system (PlantDi-Tech, Israel), following the methods described by Halperin et al. (2017) and Dalal et al. (2020). Briefly, plant weight gain(g) was calculated every day at the end of each irrigation and drainage period, at pre-dawn (ΔPW). The system automatically accomplished this by comparing pot weights (after subtracting all tare weights) upon drainage termination when the soil reached field capacity on consecutive days. Plant daily transpiration (PDT, g day^{-1}) was calculated every day as the weight difference between pre-dawn and few minutes before the first irrigation at night. The whole-plant WUE during a defined period was determined by the ratio between the sum of the daily plant fresh-weight gain (ΔPW) and water used throughout this period:

$$WUE = \frac{\sum \Delta PW_n}{\sum PDT_n} \quad (1)$$

Eq. (2) was then used to determine plant weight gain during the drought period, when plants were not irrigated, and the above procedure could not be applied.

$$\sum \Delta PW_n = WUE \cdot \sum PDT_n \quad (2)$$

WUE was calculated for the well-irrigated period (Eq. 1), and PDTn is the measured daily water consumption throughout this period, where n is the number of days measured. Plant agronomic water-use efficiency, WUE (WUEb; gbiomass/gwater), was calculated by dividing the dry biomass weight (g; measured at the end of the experiment) by the cumulative transpiration of each plant (gwater) over the entire experimental period. The momentary whole-plant transpiration rate (Tr; gwater·min^{-1}) was derived by multiplying the first derivative of the measured load-cell time series by –1. Tr was then normalized by plant fresh weight to yield Ec (gwater ·gplant^{-1}min^{-1}).

The whole-canopy conductance (G_{sc}) was calculated using Eq. (3)

$$Gsc = Ec \cdot BP \cdot VPD^{-1} \quad (3)$$

where VPD is the vapor pressure deficit (kPa) and BP is the atmospheric barometric pressure (kPa). Thus, Gsc is expressed in units of $g_{water} \cdot g_{plant}^{-1} min^{-1}$ (Halperin et al., 2017).

Before these calculations, the time-series data were smoothed using the Savitzky–Golay method with a 61-point filter window and a fourth-order polynomial. This step was taken to mitigate noise amplification, which increases as the sampling interval decreases.

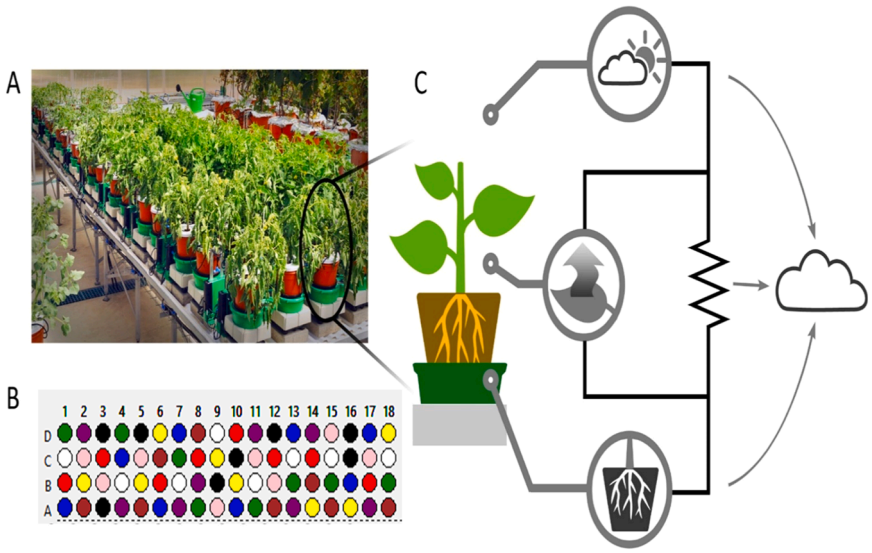

Fig. 1. Overview of the telemetric, gravimetric phenotyping platform and analysis scheme. A, A partial view of multiple tomato introgression lines positioned on the Plantarray screening platform [located at the Israeli Center of Research Excellence (ICORE) for Plant Adaptation to the Changing Environment, at The Hebrew University of Jerusalem]. B, randomized experimental setup of all plants simultaneously measured. Different colors represent different lines and treatments. C, An illustration of the direct soil-plant-atmosphere measurements taken for a single plant.

2.7. Gas exchange measurements

Leaf gas-exchange was assessed on the youngest, fully expanded leaf. Measurement data were collected from mature, fully expanded leaflets at the top of the canopy of ~8-week-old plants between 10:00 am and 12:00 pm. A portable infra-red gas analyzer (LI-6800XT; Li-Cor Inc., Lincoln, NE, USA) was used to obtain the carbon assimilation rate (A_N). Stomatal conductance (g_s) was measured in a 6 cm^2 chamber, at midday, with the CO_2 reference set at 400 ppm (μmol mol^{-1}), PPFD at 1400 μmol m^{-2} s^{-1}, VPD at 1.4 kPa and temperature set at 25°C. Those levels were selected to replicate the greenhouse environmental conditions at the time of the initial measurements.

2.8. Stomatal density and aperture

Stomatal apertures and density on both leaf surface were determined using a rapid imprinting method (Geisler and Sack, 2002), widely used with fast-drying (~1 min) (Attia et al., 2015a), light-bodied vinyl polysiloxane dental resin (Heraeus-Kulzer, https://www.kulzerus.com). Measurements were taken on the main lamina areas, avoiding major veins and vein-associated tissues to ensure consistency and accuracy. The vein areas were excluded by carefully selecting interveinal regions for analysis, following standard protocols to minimize variability and ensure representative sampling of stomatal distribution. The dried resins were used to create positive impressions with transparent nail polish, which were then transferred onto a microscopic slide. All stomata were then photographed using a bright-field inverted microscope (Nikon Eclipse TS100, Japan) with a 20 × /NA 0.40 objective and a 12-bit CCD camera (Manta G-235B; https://www.alliedvision.com). Stomatal aperture was measured directly from the pore dimensions visible in the imprints, thereby capturing pore geometry at the moment of fixation. We interpret this as an anatomical snapshot of aperture at fixation, not as a direct equivalent of functional stomatal openness or stomatal conductance. This allowed us to collect large samples of stomatal imprints (see Suppl. Fig. 4). For uniformity of sampling, we imprinted stomata from the youngest fully expanded trifoliate leaves exposed to full sunlight and obtained images of approximately four randomly selected areas on the leaf, avoiding major veins and vein-associated tissues. The images were analyzed using ImageJ, with a calibrated microscope ruler used for size calibration.

2.9. Statistical analysis

Unless otherwise specified, all statistical analyses were performed using JMP ver. 15 statistical package (SAS Institute, Cary, NC, USA). Analysis of variance (ANOVA) was calculated, and subsequent comparisons were analyzed using Tukey's *post hoc* test. A p-value of ≤ 0.05 was considered statistically significant for the ANOVA tests. The specific statistical tests used are indicated in the legends of each figure or table. Graphs were generated using OriginPro, Version 2021 (OriginLab Corporation). Correlation analyses were performed in the R Statistical package's cor() function, which computes pairwise correlation coefficients for continuous variables.

3. Results

3.1. Field performance of the IL population

We began by analyzing two field experiments conducted in 2000 and 2004 (see Table 1) that included 29 IL lines and M82. These plants were characterized by yield and biomass parameters and compared to the control M82 under optimal and water-limiting conditions (Fig. 2). The percentage change in biomass and fruit yield was calculated relative to M82, a "check variety". Under optimal irrigation, the lines were classified into high-yield (HY), medium-yield (MY), and low-yield (LY) groups based on their yields relative to M82: HY = >20% greater than the yield of M82, MY = yield levels comparable to, but not necessarily equal to, that of M82, and LY = 20% lower than the yield of M82. Based on the biomass of the different lines collected from the field at the experiment's end relative to M82, the genotypes were also classified as having high shoot biomass (HB, >20%), medium shoot biomass (MB, =20%), or low shoot biomass (LB, <20%; Table 1) as compared to the biomass of M82.

Six lines (marked with *in Table 1) with a range of low to high biomass and fruit yield, and the M82 line, were chosen for further physiological characterization using the functional phenotyping platform to dissect the physiological basis of their difference. These six genotypes were selected to represent a broad range of plant response characteristics, based on data from 4 to 5 years of well-irrigated field experiments and at least two years of data on performance under stress conditions. The selected lines were IL5–2, IL11–4, IL2–6, IL8–1, IL10–1, and IL8–1–3. Among these lines. IL5–2 outperformed M82 in all

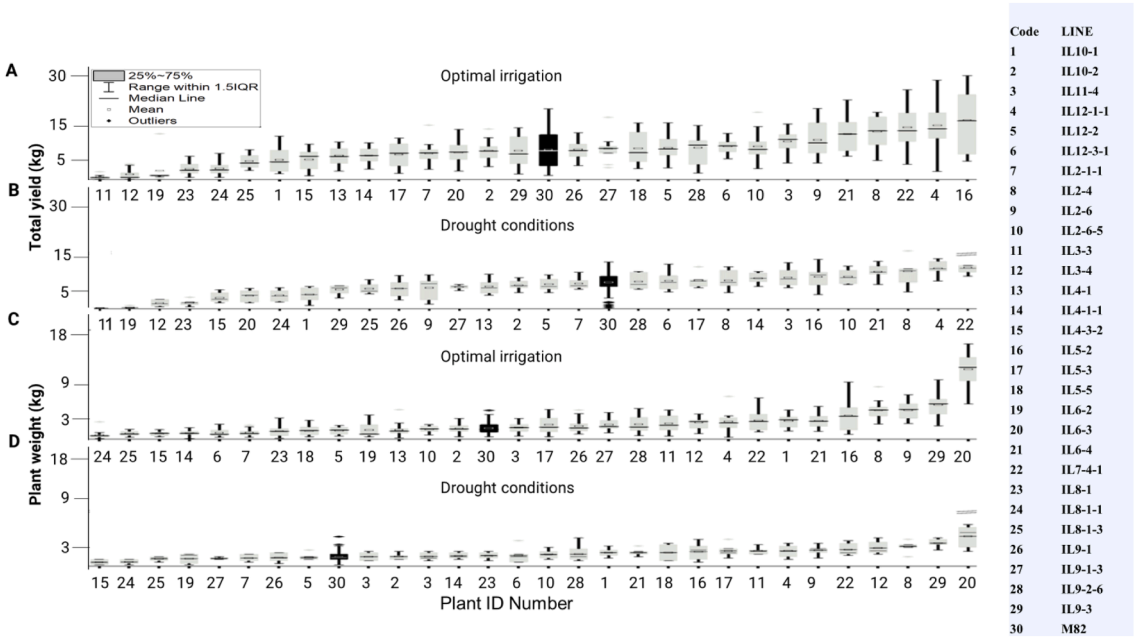

Fig. 2. Field performance of 29 tomato introgression lines (gray) and the M82 control (black). A, Two years of mean fruit weights (ranked from low to high) under well-irrigated conditions. B, Two years of mean fruit weights (ranked from low to high) under drought conditions. C, Two years of mean shoot weights at harvest (ranked from low to high) under well-irrigated conditions. D, Two years of mean shoot weights at harvest (ranked from low to high) under drought conditions. The square (□) in the box plot represents the mean value. The box-splitting horizontal bands indicate the sample median, and bars show the interquartile range (25th to 75th percentile). Points below or above the interquartile ranges are outliers, respectively(n = 9–13).

parameters in both environments; thus, we classified the HY, HB, HT, and HR (HyHbHtHr) line as ideotypic. IL2–6 was a high-yield under optimal irrigation but a low-yield under drought stress, while maintaining high biomass under both conditions (HyHbLtHr). IL11–4 exhibited high yields under optimal irrigation but had medium-level values for the other selection criteria (HyMbMtMr). IL10–1 exhibited robust vegetative growth but yielded low amounts in wet and dry conditions. It was characterized by a low yield, high biomass, low tolerance, and high resilience (LyHbLtHr). IL8–1 had low total yields and biomass under optimal irrigation and low yields under drought conditions, but medium biomass under drought stress (LySbLtMr). IL8–1–3 had low total yields and biomass under optimal irrigation and low yields under both optimal irrigation and drought conditions (LySbLtLr). Physiological characterization of the selected introgression lines

As a preliminary approach, we conducted single-time- point measurements of stomatal conductance and photosynthesis using a widely adopted IRGA gas-exchange system (Supplementary Figure 3). However, these single-time-point measurements did not reveal statistically significant differences among the introgression lines. We attribute this to substantial biological and environmental variability across replicates, likely driven by fluctuations in light intensity, temperature, and vapor pressure deficit (VPD) during the measurement period required to cover all plants sequentially. Thus, although chamber conditions were standardized, the plants were not measured simultaneously and their physiological state varied across an approximately 2 h time window and greenhouse microclimate. This underscores that single-time-point IRGA measurements have limited power to resolve genotype differences in diurnal water-use dynamics, thereby motivating our continuous whole-plant approach.

This limitation inherent to manual gas-exchange systems prompted us to employ a high-resolution gravimetric phenotyping platform capable of continuously and simultaneously monitoring whole-plant transpiration. This system enabled the detection of dynamic physiological patterns across genotypes under identical and gradually changing drought conditions.

During continuous, simultaneous measurement of whole-plant physiological performance, all lines showed linear increases in transpiration under optimal irrigation. When comparing whole-plant daily transpiration, no significant differences were observed between the lines on the first experimental day (4-week-old seedlings) (Fig. 3B, Day 1). From 2–17 days after transplanting, IL11–4 and IL5–2 showed significantly higher whole-plant transpiration than the Check variety (M82), whereas IL8–1 exhibited moderate to lower transpiration relative to the Check variety. After 18 days, all plants underwent controlled drought stress (a differential-feedback-irrigation drought treatment; see Materials and Methods), ensuring they experienced a similar drought stress, in which the soil volumetric water content (VWC) decreased at a similar rate (Fig. 3B), despite differences in transpiration. Although all plants encountered a similar declining VWC, high-transpiring lines reached their VWC limitation point (θcrit) more swiftly, thus reducing their transpiration rate earlier than the low-transpiring plants (Fig. 4, Suppl. Figure 2), revealing a transpiration-positional inversion (e.g., Fig. 3B, the transpiration “flip-flop” of IL11–4 and IL8–1).

3.2. *Stress response and resilience evaluation*

During the drought period, no differences in plant transpiration were observed between the lines (Fig. 3B). We therefore assessed recovery rates (resilience) of the different lines after full irrigation was reinstated, once plant transpiration had declined to approximately 10% of their maximum transpiration (Day 29). The transpiration was measured until the plants returned to their previous (non-normalized) transpiration rates observed before the drought stress. Over this period, all lines recovered successfully to their pre-stress transpiration levels. However, the high-transpiring line (IL5–2) exhibited a faster absolute recovery rate (as measured by actual, whole-plant water-loss rates, which were not normalized; Fig. 5A) than the low-transpiring lines (IL8–1 and IL2–6), suggesting more effective drought-response and resilience mechanisms. We assumed that plants with higher transpiration rates would be more negatively affected by drought. However, it was notable that high transpiration was coupled with greater resilience. In addition, we observed a strong correlation between cumulative transpiration (CT)

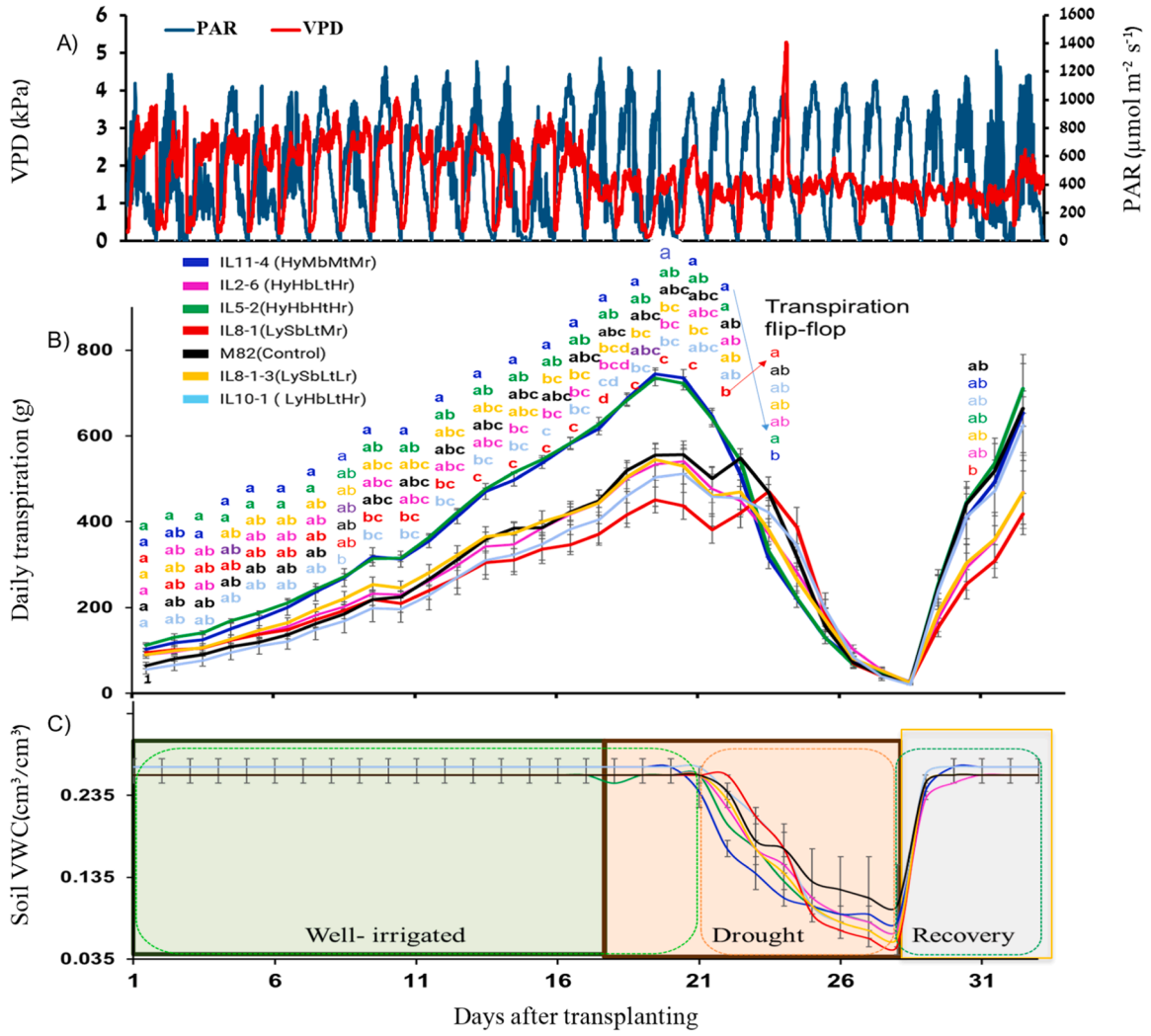

Fig. 3. A, Daily photosynthetically active radiation (PAR) and vapor pressure deficit (VPD) during the experimental period. B, Daily transpiration of tomato seedlings over the entire experimental period. Data points are means ± SE of continuous daily whole-plant transpiration over the entire experimental period (32 days). C, mean ± SE volumetric water content (VWC) measured by a soil probe over the course of the experiment. The drought treatment was followed by a recovery period during which the resumed irrigation brought the pot back to full capacity. Groups were compared using Tukey's Honest Significance test; different letters above represent significant differences between lines; $p < 0.05$. $n = 5$–8 plants per group.

and dry biomass at harvest (Fig. 5B, r^2=0.89). Moreover, the lines with higher CT (IL5–2 and IL11–4) exhibited higher transpiration-use efficiency (transpiration normalized by biomass; WUEb), with IL11–4 showing significantly higher WUEb than IL8–1 ($P < 0.05$), indicating improved water-use efficiency mechanisms in these high-transpiring lines (Fig. 5C).

3.3. Daily whole-plant–environment kinetics

Single-point measurements of daily transpiration parameters can be challenging to compare plant performance because plants respond dynamically to microclimate factors, such as fluctuating light, temperature, and vapor pressure deficit (VPD). The high signal-to-noise ratio of the system (see materials and methods) enables the precise measurement of momentary transpiration rates rather than just daily aggregates, ensuring continuous monitoring and analysis of transient physiological responses. Therefore, we could measure differences in the momentary plasticity response to ambient conditions throughout the day, which might provide additional explanations for the performance differences between lines. To comprehend the response of Gsc and the transpiration rate to ambient conditions, we monitored all lines simultaneously under optimal irrigation and similar soil water content conditions (50% of maximum midday transpiration, after θcrit, day 23 of the experiment; this stress level synchronization (Fig. 3C) was possible due to the system's automatic feedback irrigation control, see Materials and Methods). Under well-irrigated conditions (Day 16 of the experiment), the whole-canopy Gsc and TR exhibited similar response patterns to light and VPD across lines. All lines opened their stomata in response to PAR and VPD, increasing their Gsc and TR from 06:00–10:00 (Figs. 6B and 6C). Daily maximum Gsc and TR increased in parallel with rising PAR and VPD during the early morning hours, stabilizing around 10:00 AM, after which both environmental and plant physiological parameters remained relatively constant throughout midday and into the late afternoon (10:00–16:00). In the late afternoon, Gsc sharply declined in response to PAR, while TR remained high following the VPD pattern. With the VPD drop (Fig. 6A), transpiration also decreased (Fig. 6C). Similar findings have been reported by (Fridman et al., 2000), who found that canopy photosynthesis increased rapidly, reaching a high level shortly after sunrise. In contrast, transpiration increased slowly following the VPD trend, ultimately resulting in a high canopy of WUE accompanied by high carbon assimilation before 7:00. This observation suggests the possibility that the plants' WUE might have been at its lowest during the afternoon and evening hours; however, further measurements normalizing transpiration to biomass or photosynthetic rates would be required

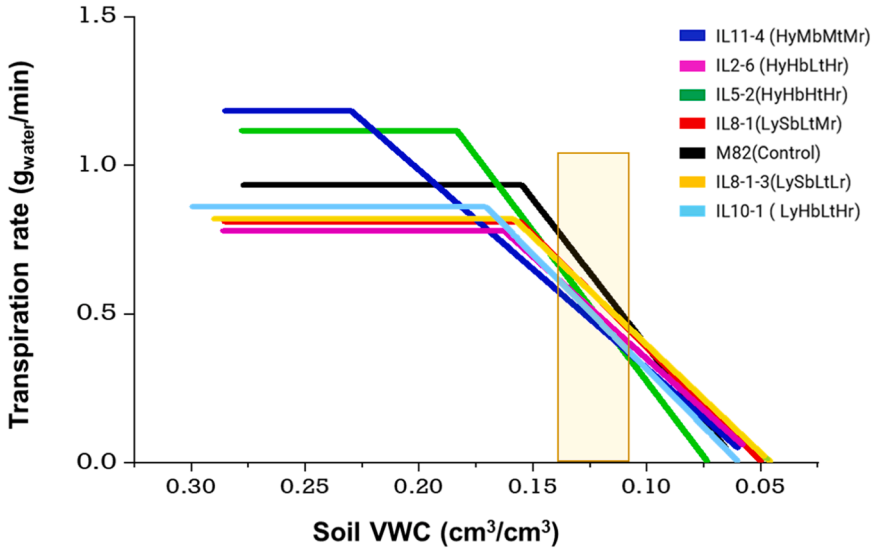

Fig. 4. The physiological drought point (θcrit) was determined as the point at which soil water is restricted from supplying mid-day transpiration needs, for all the plants presented in Fig. 3. This point was identified using piecewise correlations based on the relationships between two segmented lines that intersected (following Halperin 2016). The yellow box in the middle represents the standard drought-evaluation zone, in which the performance of all lines was evaluated under drought stress.

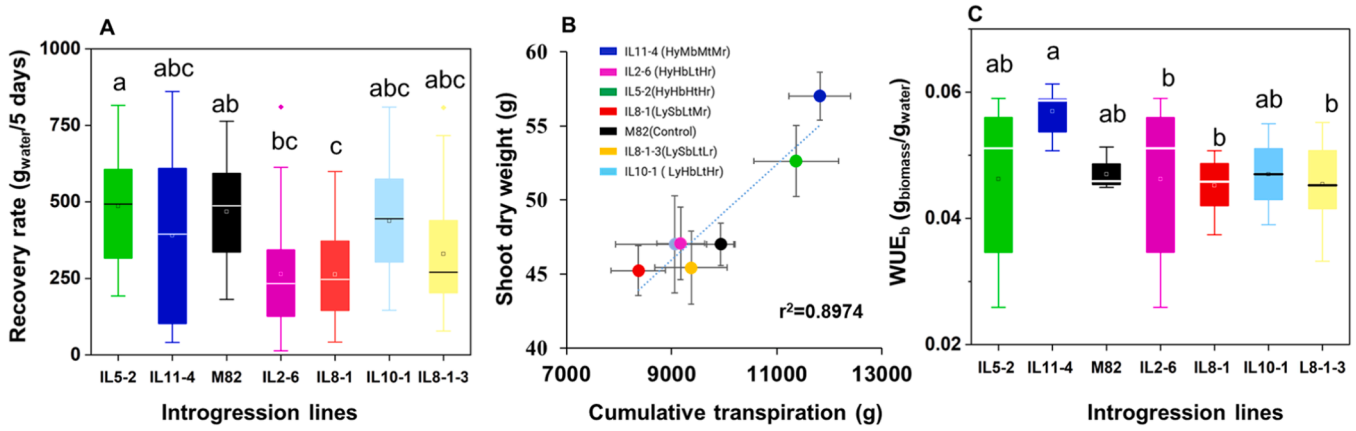

Fig. 5. A, Transpiration recovery rate for five days after the resumption of irrigation in seven different tomato lines. B, Correlation between shoot dry weight and cumulative daily transpiration for 33 days during the screening period. Data points are the means ± SE ($n = 5$—8). C, means ± SE of biomass WUE of the different lines. Different letter indicates significant difference according to Tukey's Honest Significance test ($p < 0.05$).

to confirm this speculation. The maximum midday transpiration rate displayed a pattern similar to the daily transpiration trend presented in Fig. 3, with consistent differences among lines. However, when normalized by plant biomass and VPD to obtain canopy conductance (Gsc), a different pattern emerged, characterized by an early morning peak followed by a decline during midday and the afternoon hours. Unlike under optimal irrigation conditions, the Gsc and TR kinetics of plants exposed to soil water-limiting conditions varied among lines and in response to PAR and VPD (which were very similar to the pre-stress conditions; see Supplemental Figure 1). All lines experienced reductions in Gsc and TR from late morning to noon, regardless of the ambient PAR and VPD conditions. However, the high-performing lines (i.e., IL5–2 and IL11–4) exhibited a distinct response pattern, characterized by an early-morning peak in Gsc (Fig. 7 A and B) and a relatively low transpiration rate (Fig. 7a and b) at the same time, followed by an immediate and linear reduction in those parameters during the middle of the day and the afternoon (10:00 to the evening hours).The differential sensitivity of transpiration (Tr) to vapor pressure deficit (VPD) and stomatal conductance (g_s) to light is consistent with established stomatal control mechanisms, whereby VPD directly influences evaporative demand while light regulates stomatal opening through photosynthetic signaling pathways (The control of stomata by water balance - Buckley, 2005; Farquhar and Sharkey, 1982). This pattern can be interpreted in the context of photosynthetic feedback on stomata, where changes in mesophyll photosynthesis and intercellular CO_2 concentration modulate g_s, linking light-driven carbon assimilation to stomatal behavior (Wong et al., 1979; Lawson et al., 2012). Conversely, low-performing lines (i.e., IL10–1, IL8–1, and IL8–1–3) presented lower Gsc during the early hours (when VPD is low). They reached their Gsc peaks later in the day (Fig. 7 E, F, and G, respectively). Those peaks persisted for longer periods, causing those plants to lose more water through transpiration (Fig. 7e, f, and g, respectively). Importantly, all measurements in Fig. 7 were conducted on the same day under the same VPD trajectory and at similar soil water content levels (Figs. 3B and 4), ensuring comparability across lines. In these high-resolution measurements of continuous Gsc and Tr patterns, we detected differences between lines that were not evident in the low-resolution measurements of single-point daily transpiration (i.e., no differences between lines were detected in the daily-transpiration stress response, unlike the pre-stress period; Fig. 3A). To better understand the different Gsc response

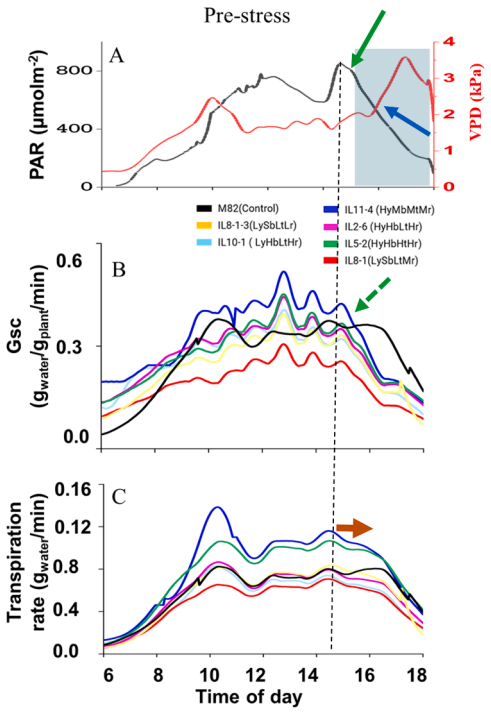

Fig. 6. Daily patterns of A, PAR (black line) and VPD (red line), B, whole-canopy conductance, and C, whole-canopy transpiration rate, as continuously measured under well-irrigated conditions. The green solid line arrow shows a sharp decline of PAR; the blue solid arrow indicates an Increase of VPD. The green broken arrow suggests a sharp decrease in GSc, and the orange solid arrow indicates when transpiration remains higher relative to GSc. Data means ± SE; $n = 5–8$.

patterns of the high-yielding lines, we examined their abaxial/adaxial stomatal densities and daily apertures.

3.4. Variation in stomatal morphology among the lines

Stomatal density and aperture (pore width) measurements revealed that lines IL5–2, IL11–4, IL8–1–3, and IL10–1 had higher abaxial than adaxial stomatal densities. In contrast, the other lines had similar stomatal densities on both leaf sides. No differences were observed in the maximal stomatal aperture size between the abaxial and adaxial leaf sides for each line, except for M82 and IL8–1–3, which had larger stomatal apertures on the abaxial and adaxial sides of their leaves, respectively (Fig. 8 B). However, each line had a maximum aperture on both the abaxial and adaxial sides of its leaves at different times of day (Fig. 9; all measurements were conducted on the same day under the same VPD and soil water content, ensuring consistency across experimental conditions). Specifically, IL5–2 reached its maximal abaxial peak aperture around 07:00 and its maximal adaxial peak aperture around 10:00 (Fig. 9 A, a). M82 reached both its maximal abaxial and adaxial apertures around 10:00. Lines IL8–1, IL11–4, and IL10–1 revealed maximum aperture on both their adaxial and abaxial sides around 13:00. However, while the stomatal apertures of IL10–1 and IL 11–4 shrank after peaking, IL8–1 maintained its large apertures until 17:00. Line IL8–1–3 consistently maintained small apertures throughout the day (Fig. 9 G and g). The aperture for line IL8–1–3 did not align well with our observations of canopy-level conductance, which may be due to single-point leaf-level aperture measurements compared with integrated whole-plant conductance data. Thus, stomatal aperture patterns (Fig. 9) reveal relatively good correspondence between the abaxial and adaxial leaf sides. Generally, the stomatal aperture patterns align well with the canopy-level conductance trends. However, some discrepancies were evident, such as in line IL8–1–3, where stomatal aperture patterns did not fully correspond to canopy-level measurements. These discrepancies might arise from methodological limitations of single-point stomatal aperture measurements compared with continuous measurements of whole-plant canopy conductance, or from other factors, such as boundary-layer effects. These aspects require further investigation.

To clarify trait associations, we quantified relationships between stomatal traits, water-use traits, and biomass using Pearson correlations across genotypes ($n = 7$, Supplementary Table S3). Cumulative transpiration (CT), an integrated whole-plant trait measured continuously across the stress and recovery period, showed strong associations with both biomass ($R^2 = 0.85$, $p = 0.003$) and post-drought recovery (CT vs. Drought_Recovery, $R^2 = 0.85$, $p = 0.003$). In contrast, agronomic WUEb and stomatal density traits showed weak, non-significant associations in this panel, including a weak association between the abaxial: adaxial stomatal density ratio and WUEb ($R^2 = 0.035$, $p = 0.689$; Supplementary Table S3).

4. Discussion

Sampling longitudinal traits, traits measured repeatedly, is crucial to understanding how the environment impacts plant performance (Yang et al., 2006). Continuous measurements have been proven to enhance the accuracy of prediction models for plant growth and to identify loci related to growth trajectories (Campbell et al., 2019). Monitoring the soil-plant-atmosphere continuum provides more informative data than single-point measurements (Moshelion et al., 2024). Under stress, plants shift from productive to survival modes, adapting physiologically, anatomically, and biochemically (Kerchev and Van Breusegem, 2022). Understanding these dynamics under water-deficit conditions, particularly in breeding for higher yields, is critical (Sinclair, 2011; Snowdon et al., 2021). The challenges of using prolonged irrigation halts to study drought stress highlight the variability of plant transpiration and the need for careful management of soil water levels, as illustrated by the method developed by (Snow and Tingey, 1985). Nevertheless, it is challenging to accurately predict the extent of time savings in the pre-cultivation process that might be achieved through novel biological or technological developments. Nonetheless, a considerable portion of the current effort is spent identifying lines that ultimately prove unsuitable for specific environmental conditions. If these unsuitable lines can be screened out at an earlier stage, both time and financial resources can be conserved, allowing more suitable candidates to advance to field testing earlier, advancing physiological trait discovery for crop improvement. In our study, we automatically maintained similar drought treatments for all lines simultaneously (Fig. 3C) using each plant's own transpiration as a feedback irrigation method to its own pot. In addition, we define the initial drought-stress point in terms of each plant's θcrit as a standard drought evaluation point (Fig. 4, Suppl. Figure 2). Thus, θcrit reveals the soil water content, which serves as a limiting factor to transpiration and how quickly plants can reduce their transpiration after reaching the θcrit point, potentially impacting their stress tolerance (Negin and Moshelion, 2016) (Gosa et al., 2019). For instance, as shown in Figs. 3B and 4 and Suppl. Figure 2, IL5–2 and IL 11–4 reached the θcrit point more rapidly than other lines. This suggests that the lines transpiring more under full irrigation (high productive mode) will reach their limiting water content faster, thus quickly closing their stomata (switching to protective mode). Such kind of transpiration observed by IL 11–4 is similar to a 'riskier' water use strategy under stress conditions (Tardieu and Simonneau, 1998), (Attia et al., 2015b); (Gosa et al., 2019) as IL 8–1 showed more conservative water use behavior, which is less productive yet might contribute to better chances to survive longer stress. While some of the differences between the lines in their soil moisture may be subtle, the patterns remain biologically meaningful and consistent with other traits. A "riskier" water-use strategy (higher transpiration under stress) generally supports higher short-term carbon assimilation, which can translate into greater early biomass accumulation and potentially higher yield if water remains

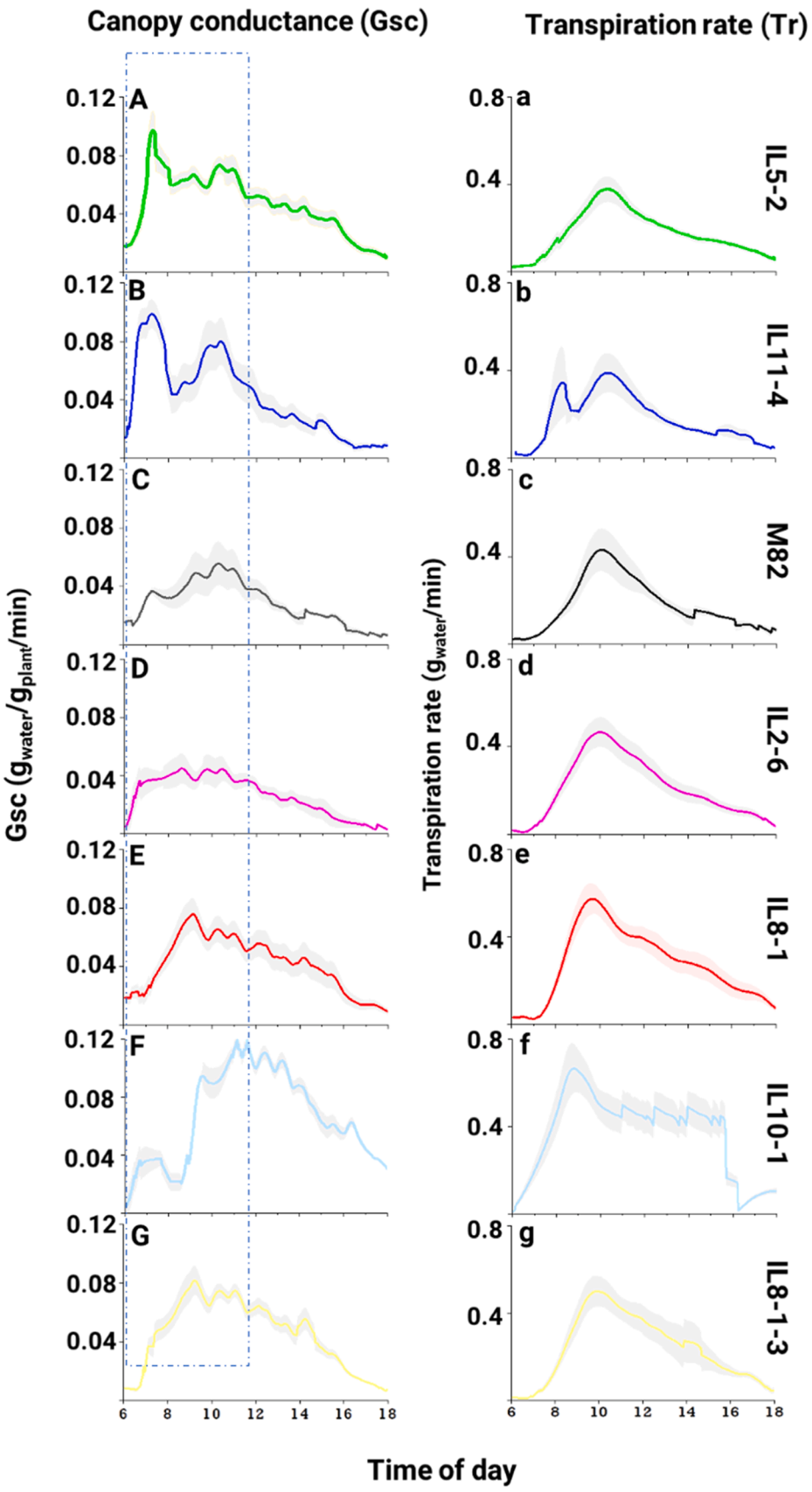

Fig. 7. Daily variation in canopy conductance and transpiration rate under drought-stress conditions. Whole-canopy conductance (A–G) and transpiration rate (a–g) were measured continuously. Representative days were shown for the stress after the θcrit point (yellow block in Fig. 4). Data was collected on the same day under a shared VPD trajectory. Additionally, the soil water content was similar across lines at the time of measurement. The broken-line box indicates the morning hours during which the stomatal peak is observed in some lines. Data are shown as means ± SE (n = 5–8). The light shadow area shows the standard error bar.

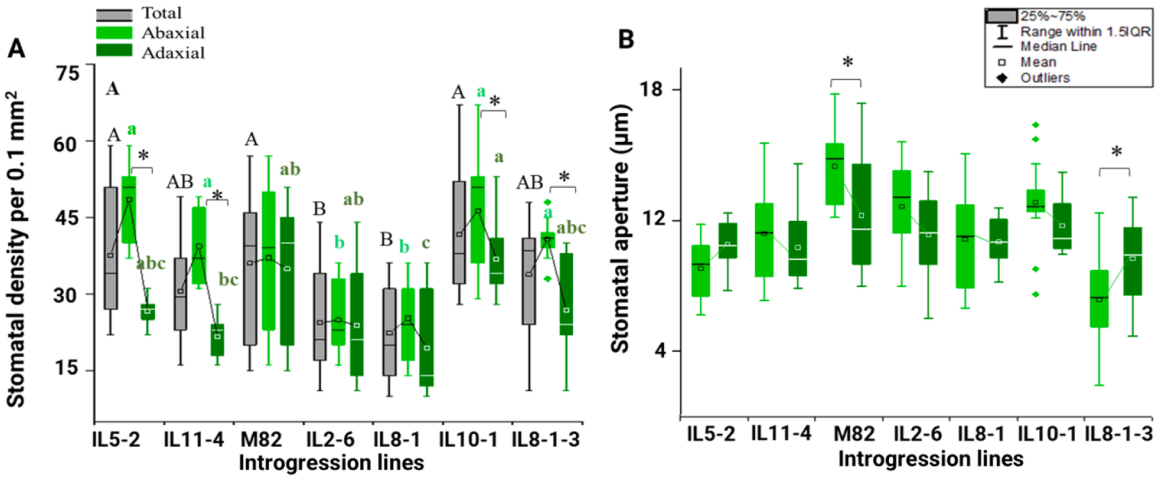

Fig. 8. Leaf stomatal traits of the different tomato lines. A, Total (gray), abaxial (lower leaf side, light green) and adaxial (upper leaf side, dark green) stomatal densities of six introgression lines of tomato and M82. Data are derived from three technical and three biological replications imaged at their central lamina. The box-splitting horizontal bands indicate sample medians, the square box in the middle indicates the mean, and bars show the interquartile range (25th to 75th percentile), points below or above the interquartile ranges are outliers. B, Total stomatal apertures of the same lines (pore width, μm). * Indicates a significant difference between the abaxial and adaxial sides of an individual line, according to Student's *t*-test. Different letters indicate significantly different means (capital letters for total stomatal density, and light green lower-case letters for the abaxial side of the leaves and dark green lower-case letters for the adaxial side), according to Tukey's Honest Significance test ($p < 0.05$, n = 8).

available through critical developmental stages. However, because this strategy accelerates soil water depletion, it increases the probability of premature water limitation during reproductive phases, which can reduce final biomass partitioning to grains and depress yield under prolonged or terminal drought(Blum, 2009). Conversely, a conservative water-use strategy typically results in lower instantaneous biomass production due to reduced gas exchange, but it preserves soil moisture for longer periods, which can stabilize yield under extended stress by maintaining plant function during sensitive growth stages (Blum, 2009; Passioura, 2012).

Recovery from drought stress entails returning to pre-stress growth and physiological functioning levels once soil water content is restored. Although resilience is as vital as the stress response, it has garnered less attention, possibly due to challenges in its characterization (Guo et al., 2020). In Fig. 5A, the lines exhibited varying abilities to revert to their pre-stress daily transpiration levels compared with their daily transpiration during the first five days after resuming irrigation following the drought treatment (Fig. 3B). Under the severe drought stress conditions (plants transpiring at less than 10% of their maximal transpiration), we expected that slow recovery due to drought-related damage (e.g. leaf and root desiccation, embolism, photorespiration, and reactive oxygen species - ROS) would more severely impact plants with higher transpiration rates and rapid growth compared to plants with lower transpiration rates and slower growth. Interestingly, lines with higher pre-stress transpiration levels (IL5–2, IL11–4) recovered swiftly after the drought, contradicting our hypothesis. Similarly, these lines were classified as highly resilient and medium resilient, respectively, under the field conditions (Table 1). They exhibited faster stomatal closure (Fig. 7A, B), high WUEb (Fig. 5C), and relatively high Gsc to TR under drought conditions (Fig. 7 A,b, and B, b, respectively). Based on these findings, we infer that stress-adaptation mechanisms, which might be elusive during the stress period, contribute to plant resilience. This aligns with a previous report on maize (Chen et al., 2016), which posited that drought recovery is integral to whole-plant growth under water-stress conditions. Employing a method to detect drought-stress resilience during early growth stages, combined with field trials, may enable predicting resilience at earlier stages. This approach could also help identify genetic variability in novel tolerance mechanisms.

4.1. Dynamic water-use efficiency: the morning stomatal peak under water-deficit conditions

Plants exhibit dynamic water-use regulation throughout the growing season in response to changes in VPD. The temporal dynamics of water-use traits can significantly enhance productivity (Sinclair, 2018). Under limiting SWC, different lines exhibited distinct responses to VPD and PAR (Fig. 7 and Supplemental Figure 1), suggesting that certain dynamic reactions may be more advantageous in specific environments. A notable example of such beneficial dynamic responses is the early-morning whole-canopy conductance peaks observed in high-yielding lines. Under drought conditions, IL5–2 and IL11–4 (Figs. 7A and 7 B) maintained relatively high whole-canopy conductance despite a still low VPD when PAR was high. This resulted in a relatively low rate of water loss via transpiration (Figs. 7a and 7b). A morning peak of this nature was reported in *solanum penelli* (Lupo and Moshelion, 2024).

Such opportunistic stomatal behavior has been documented in highly water stress-tolerant forest plants like Acacia and hemiparasitic mistletoes (*Loranthus europaeus* (LE)) (Ullmann et al., 1985; Resco de Dios et al., 2016), wheat (*Triticum durum cv*) introgression line (Bacher et al., 2023), soybean (Glycine max) (Teare and Kanemasu, 1972), and *Arabidopsis thaliana (*Hassidim et al., 2017*)*. While these studies acknowledged the existence of this stomatal morning-rise phenotype, it was hypothesized that this phenotype would enhance productivity and fitness under drought by using photosynthetically active radiation (PAR) to increase CO2 assimilation (Schoppach et al., 2020). In a recent study, we demonstrated that this type of early-morning Gsc peak, referred to as the "golden hour"(Gosa et al., 2019) , is strongly correlated with tomato yield in the field (Gosa et al., 2022b). Our current findings underscore the significance of this early-morning stomatal peak under water-limiting conditions and highlight genetic variability underlying this crucial trait. Specifically, the two high-yielding lines were IL5–2 and IL 11–4, which are otherwise distinct. Moreover, these lines exhibited high WUEb, high shoot dry weight (Fig. 5B; $P < 0.05$), and medium to high field drought tolerance (Table 1), confirming that lines that balance and optimize water use tend to maintain high productivity even under water-stress conditions. In contrast, IL2–6, which exhibited high yield under well-irrigated conditions but low yield under field drought conditions, displayed daily Gsc kinetics similar to those of the low-yielding

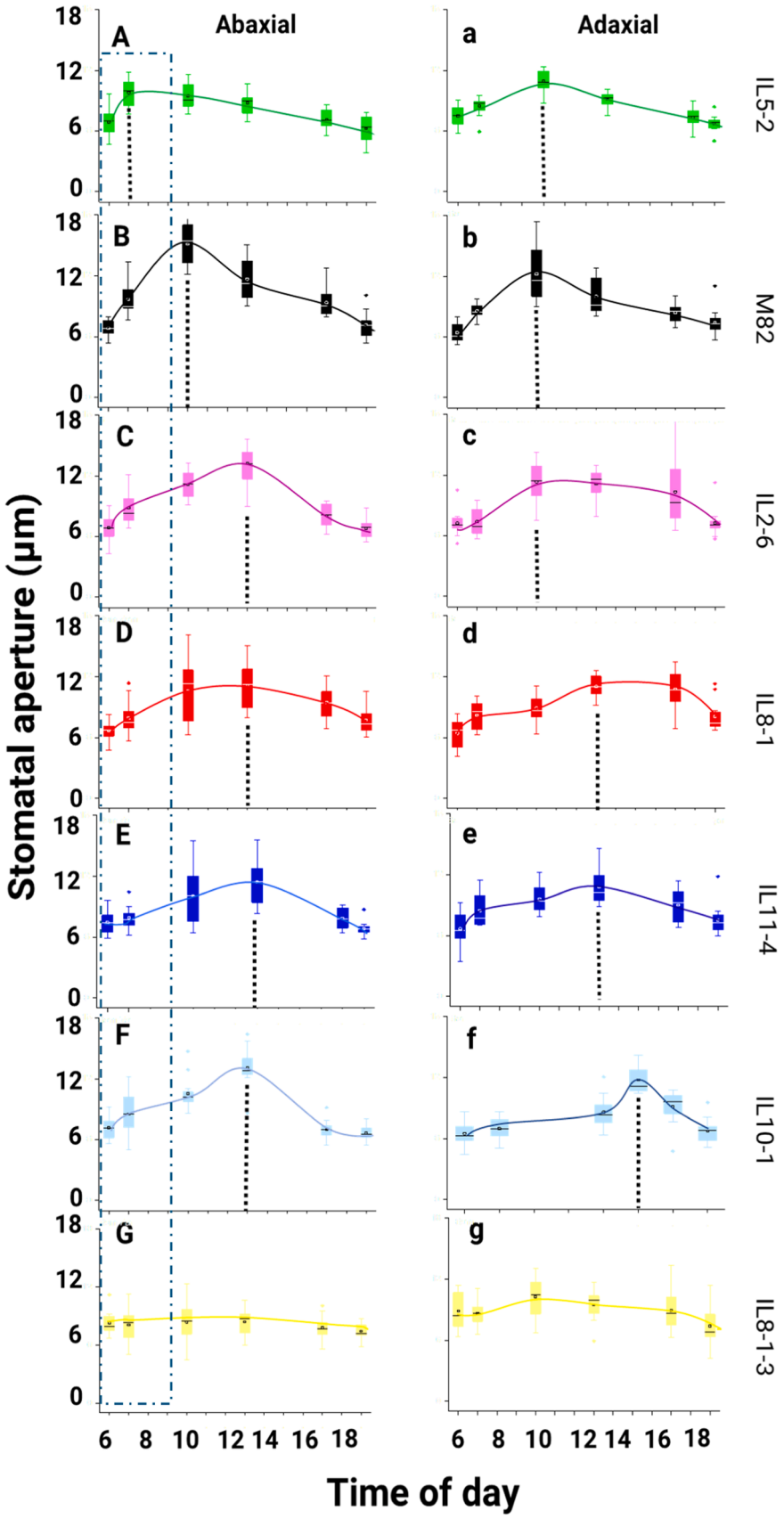

Fig. 9. Daily variation in A–G, abaxial stomatal apertures, and a–g, adaxial stomatal apertures. The broken lines indicate the morning time when the maximum aperture was observed for some of the lines. The square (□) in the box plot represents the mean value. The box-splitting horizontal bands indicate sample medians, and bars show the interquartile range (25th to 75th percentile). Points that fall below or above the interquartile ranges are considered outliers. The dashed lines in each figure indicate the point on the day at which the apertures were largest(n = 8).

IL8–1 (Fig. 7). This strengthens the evidence that the Gsc morning peak is an essential yield-related trait under stress. Furthermore, IL2–6 demonstrated low WUEb and low shoot dry weights (Fig. 5B, $P < 0.05$) and poor drought tolerance in the field (Table 1), suggesting that high yield does not necessarily indicate drought tolerance. Thus, different combinations of traits yielded similar outcomes. Although midday depression was not directly observed, it is relevant to consider that many species exhibit a midday decline in photosynthesis and stomatal conductance under high light and vapor pressure deficit, driven by stomatal and non-stomatal limitations, including, biochemical, photochemical, anatomical, and hydraulic constraints which can restrict photosynthesis even when stomata relatively are open and CO_2 is available (Henry et al., 2019; Muir et al., 2014). This framework may help contextualize diurnal patterns discussed here.

Several recent studies have proposed stomatal functional anatomy mechanisms as promising targets for enhancing productivity and resilience (Sadok et al., 2021). For instance, high stomatal density has been suggested to represent a safety-efficiency trade-off, as it shows greater sensitivity to closure during leaf dehydration (Henry et al., 2019). Another mechanism proposed as a good proxy for productivity, and WUE, is the ratio between the stomatal densities on a plant's leaves' abaxial and adaxial sides (Muir et al., 2014). Notably, in our panel, the abaxial: adaxial stomatal density ratio showed only a weak, non-significant association with WUEb (Supplementary Table S3), highlighting the added value of integrating continuous whole-plant measurements when interpreting drought-response traits.

Indeed, our results support this, revealing that different combinations of densities across IL lines yield distinct water-balance regulation strategies, drought responses, and yields. Our results indicate that static stomatal density metrics are insufficient predictors of drought performance. Instead, drought response likely depends on dynamic stomatal regulation (e.g., sensitivity to VPD or ABA signaling), hydraulic conductance, and whole-plant water-use coordination rather than anatomical stomatal abundance per se

These findings prompt further questions about the roles of stomatal ratio and density in Gsc regulation. Although the abaxial stomata seem to play pivotal roles in light sensitivity, photosynthesis, and WUE (Driscoll et al., 2006), (Lei et al., 2018). The actual relative contribution of the abaxial and adaxial leaf sides to crop productivity remains ambiguous. Several factors, such as the position of light sources in the greenhouse, wind movement in the field, and crop type, influence it (Zhang et al., 2023) (Paradiso et al., 2020). We propose that, in tomatoes, the combination of stomatal ratio, stomatal density, and the sensitivity of stomata on each leaf side to ambient conditions is key to understanding a genotype's adaptation to a specific environment (G×E optimization), its resilience, and its water-use efficiency (WUE). For instance, both IL8–1 and IL8–1–3 were very low in all productive and resilient field-based parameters (Table 1).

Stomatal ratio like the high-yielding IL5–2 (Fig. 8A), but it exhibited low transpiration (Fig. 3A, $P < 0.05$) and low yield in the field (Table 1). This could be explained by the relatively small stomatal apertures on both sides of its leaves (Figs. 8B, 9G, and 9g). The stomatal density data, coupled with whole-plant canopy conductance, suggests the potential for hydraulic coupling between stomatal distribution and xylem water transport.

These aspects should be addressed in future studies to understand how abaxial vs. adaxial stomata alter leaf boundary-layer resistance, transpiration fluxes, and hydraulic signaling across the canopy. While this study differentiates between abaxial and adaxial stomatal distributions, we acknowledge that future work should aim to incorporate these parameters into a quantitative model to better capture their combined influence on gas exchange and water-use efficiency.

Unlike continuous and simultaneous canopy scale measurements, single-leaf stomatal conductance or aperture provide high spatial resolution of guard cell behavior but remain sensitive to the local microenvironment of the sampled leaf and represent a snapshot in time. In our study, single-point measurements did not show a significant difference in leaf gas exchange. All plants were measured at a similar developmental stage. Yet, because a single IRGA was used across multiple genotypes, with up to 20 min required per steady-state measurement (across a diurnal window of approximately 10:00–2:00), variability likely arises from both biological differences and fluctuations in light, temperature, and VPD over the measurement period. Such measurements do not capture spatial heterogeneity across the canopy or the temporal integration of responses under fluctuating conditions and therefore may not fully represent whole-plant gas-exchange dynamics. Accordingly, partial mismatches between leaf-level aperture patterns and canopy-level conductance (e.g., IL8–1–3) may be expected when comparing snapshot measurements to continuous whole-plant integration. Notably, an elegant solution to directly synchronize aperture dynamics with operational gas exchange has recently been demonstrated by integrating live confocal microscopy with simultaneous leaf gas exchange under controlled environmental conditions (Crawford et al., 2025). While highly informative mechanistically, this approach is not readily scalable to high-throughput phenotyping across multiple genotypes; therefore, continuous whole-plant canopy conductance remains the most practical framework for breeding-oriented screening under realistic, fluctuating conditions.

Stomatal traits contributed mechanistically to these dynamics. High-performing lines combined early-morning stomatal opening under low VPD with an elevated abaxial–adaxial stomatal density ratio, a configuration that likely favors efficient gas exchange, moderated water loss, and faster hydraulic recovery following stress release. These results support a framework in which stomatal distribution interacts with whole-plant hydraulic coordination to accelerate recovery, rather than acting as a static morphological predictor.

Integrating continuous whole-plant transpiration with stomatal morphology and aperture dynamics, therefore, enhances early phenotyping resolution and improves identification of productive, drought-resilient ideotypes. Future studies applying diverse stress scenarios and genetic dissection will be required to validate the generality of these mechanisms.

CRediT authorship contribution statement

Sanbon Chaka Gosa: Writing – review & editing, Writing – original draft, Visualization, Validation, Supervision, Project administration, Methodology, Investigation, Formal analysis, Data curation, Conceptualization. **Ravitejas Patil:** Writing – review & editing, Writing – original draft, Validation, Methodology, Investigation, Data curation. **Bogale Abebe Gebeyo:** Writing – review & editing, Writing – original draft, Validation, Methodology, Data curation. **Menachem Moshelion:** Writing – review & editing, Writing – original draft, Validation, Supervision, Resources, Project administration, Methodology, Investigation, Funding acquisition, Formal analysis, Conceptualization. **Ramón Mencia:** Writing – review & editing, Writing – original draft, Validation, Project administration, Data curation.

Declaration of Competing Interest

The authors have no conflicts of interest to declare.

Acknowledgement

This research was supported by the ISF-NSFC joint research program (grant no. 2436/18), the Israel Science Foundation (grant no. 1043/20), and the Israel Ministry of Agriculture and Rural Development (Eugene Kandel Knowledge Centers) as part of the Root of the Matter: The Root Zone Knowledge Center for Leveraging Modern Agriculture. We thank Prof. Dani Zamir at our institute for providing us with the IL seeds and multiple years of field-based yield data for the lines used in this study.

Appendix A. Supporting information

Supplementary data associated with this article can be found in the online version at doi:10.1016/j.plantsci.2026.113170.

Data availability

Data will be made available on request.

References

Tian, Z., Wang, J., Li, J., Han, B., 2020. Designing future crops: challenges and strategies for sustainable agriculture. Plant J. 105. https://doi.org/10.1111/tpj.15107.

Moshelion, M., Altman, A., 2015. Current challenges and future perspectives of plant and agricultural biotechnology. Trends Biotechnol. 33, 337–342. https://doi.org/10.1016/j.tibtech.2015.03.001.

Voss-Fels, K.P., Cooper, M., Hayes, B.J., 2019. Accelerating crop genetic gains with genomic selection. Theor. Appl. Genet 132, 669–686. https://doi.org/10.1007/s00122-018-3270-8.

Endo, H., Torii, K.U., 2019. Stomatal development and perspectives toward agricultural improvement. Cold Spring Harb. Perspect. Biol. 11, a034660. https://doi.org/10.1101/cshperspect.a034660.

Harrison, E.L., Arce Cubas, L., Gray, J.E., Hepworth, C., 2020. The influence of stomatal morphology and distribution on photosynthetic gas exchange. Plant J. 101, 768–779. https://doi.org/10.1111/tpj.14560.

Shahinnia, F., Le Roy, J., Laborde, B., Sznajder, B., Kalambettu, P., Mahjourimajd, S., Tilbrook, J., Fleury, D., 2016. Genetic association of stomatal traits and yield in wheat grown in low rainfall environments. BMC Plant Biol. 16, 150. https://doi.org/10.1186/s12870-016-0838-9.

Matthews, J.S.A., Vialet-Chabrand, S., Lawson, T., 2018. Acclimation to fluctuating light impacts the rapidity of response and diurnal rhythm of stomatal conductance. Plant Physiol. 176, 1939–1951. https://doi.org/10.1104/pp.17.01809.

Adachi, S., Tanaka, Y., Miyagi, A., Kashima, M., Tezuka, A., Toya, Y., Kobayashi, S., Ohkubo, S., Shimizu, H., Kawai-Yamada, M., Sage, R.F., Nagano, A.J., Yamori, W., 2019. High-yielding rice Takanari has superior photosynthetic response to a commercial rice Koshihikari under fluctuating light. J. Exp. Bot. 70, 5287–5297. https://doi.org/10.1093/jxb/erz304.

Ohsumi, A., Kanemura, T., Homma, K., Horie, T., Shiraiwa, T., 2007. Genotypic variation of stomatal conductance in relation to stomatal density and length in rice (Oryza sativa L. Plant Prod. Sci. https://doi.org/10.1626/pps.10.322.

McAusland, L., Vialet-Chabrand, S., Davey, P., Baker, N.R., Brendel, O., Lawson, T., 2016. Effects of kinetics of light-induced stomatal responses on photosynthesis and water-use efficiency. N. Phytol. 211, 1209–1220. https://doi.org/10.1111/nph.14000.

Battle, M.W., Vialet-Chabrand, S., Kasznicki, P., Simkin, A.J., Lawson, T., 2024. Fast stomatal kinetics in sorghum enable tight coordination with photosynthetic responses to dynamic light intensity and safeguard high water use efficiency. J. Exp. Bot. 75, 6796–6809. https://doi.org/10.1093/jxb/erae389.

Vialet-Chabrand, S., Lawson, T., 2019. Dynamic leaf energy balance: deriving stomatal conductance from thermal imaging in a dynamic environment. J. Exp. Bot. 70, 2839–2855. https://doi.org/10.1093/jxb/erz068.

Durand, M., Brendel, O., Buré, C., Le Thiec, D., 2019. Altered stomatal dynamics induced by changes in irradiance and vapour-pressure deficit under drought: impacts on the whole-plant transpiration efficiency of poplar genotypes. N. Phytol. 222, 1789–1802. https://doi.org/10.1111/nph.15710.

Gosa, S.C., Koch, A., Shenhar, I., Hirschberg, J., Zamir, D., Moshelion, M., 2022a. The potential of dynamic physiological traits in young tomato plants to predict field-yield performance. Plant Sci. 315, 111122. https://doi.org/10.1016/j.plantsci.2021.111122.

Ghanem, M.E., Marrou, H., Sinclair, T.R., 2015. Physiological phenotyping of plants for crop improvement. Trends Plant Sci. 20, 139–144. https://doi.org/10.1016/j.tplants.2014.11.006.

Dalal, A., Shenhar, I., Bourstein, R., Mayo, A., Grunwald, Y., Averbuch, N., Attia, Z., Wallach, R., Moshelion, M., 2020. A telemetric, gravimetric platform for real-time physiological phenotyping of plant-environment interactions. J. Vis. Exp. https://doi.org/10.3791/61280.

Jaramillo Roman, V., van de Zedde, R., Peller, J., Visser, R.G.F., van der Linden, C.G., van Loo, E.N., 2021. High-resolution analysis of growth and transpiration of quinoa under saline conditions. Front. Plant Sci. 12. https://doi.org/10.3389/fpls.2021.634311.

Xiong, D., Flexas, J., 2020. From one side to two sides: the effects of stomatal distribution on photosynthesis. N. Phytol. 228, 1754–1766. https://doi.org/10.1111/nph.16801.

Parkhurst, D.F., 1978. The adaptive significance of stomatal occurrence on one or both surfaces of leaves. J. Ecol. 66, 367. https://doi.org/10.2307/2259142.

Drake, P.L., Froend, R.H., Franks, P.J., 2013. Smaller, faster stomata: scaling of stomatal size, rate of response, and stomatal conductance. J. Exp. Bot. 64, 495–505. https://doi.org/10.1093/jxb/ers347.

Muir, C.D., 2015. Making pore choices: repeated regime shifts in stomatal ratio. Proc. Biol. Sci. 282, 20151498. https://doi.org/10.1098/rspb.2015.1498.

Franks, P.J., Beerling, D.J., 2009. Maximum leaf conductance driven by CO_2 effects on stomatal size and density over geologic time. Proc. Natl. Acad. Sci. U. S. A. 106, 10343–10347. https://doi.org/10.1073/pnas.0904209106.

Lawson, T., Vialet-Chabrand, S., 2019. Speedy stomata, photosynthesis and plant water use efficiency. N. Phytol. 221, 93–98. https://doi.org/10.1111/nph.15330.

Eshed, Y., Zamir, D., 1995. An introgression line population of Lycopersicon pennellii in the cultivated tomato enables the identification and fine mapping of yield-associated QTL. Genetics 141, 1147–1162. https://doi.org/10.1093/genetics/141.3.1147.

Gur, A., Zamir, D., 2004. Unused natural variation can lift yield barriers in plant breeding. PLoS Biol. 2, e245. https://doi.org/10.1371/journal.pbio.0020245.

Fridman, E., Pleban, T., Zamir, D., 2000. A recombination hotspot delimits a wild-species quantitative trait locus for tomato sugar content to 484 bp within an invertase gene. Proc. Natl. Acad. Sci. 97, 4718–4723. https://doi.org/10.1073/pnas.97.9.4718.

Halperin, O., Gebremedhin, A., Wallach, R., Moshelion, M., 2017. High-throughput physiological phenotyping and screening system for the characterization of plant–environment interactions. Plant J. 89, 839–850. https://doi.org/10.1111/tpj.13425.

Gosa, S.C., Lupo, Y., Moshelion, M., 2019. Quantitative and comparative analysis of whole-plant performance for functional physiological traits phenotyping: new tools to support pre-breeding and plant stress physiology studies. Plant Sci. 282, 49–59. https://doi.org/10.1016/j.plantsci.2018.05.008.

Dalal, A., Bourstein, R., Haish, N., Shenhar, I., Wallach, R., Moshelion, M., 2019. Dynamic physiological phenotyping of drought-stressed pepper plants treated with "productivity-enhancing" and "survivability-enhancing" biostimulants. Front. Plant Sci. 10, 905. https://doi.org/10.3389/fpls.2019.00905.

Moshelion, M., 2020. The dichotomy of yield and drought resistance: Translation challenges from basic research to crop adaptation to climate change. EMBO Rep. 21, e51598. https://doi.org/10.15252/embr.202051598.

Geisler, M.J., Sack, F.D., 2002. Variable timing of developmental progression in the stomatal pathway in Arabidopsis cotyledons. N. Phytol. 153, 469–476. https://doi.org/10.1046/j.0028-646X.2001.00332.x.

Attia, Z., Domec, J.-C., Oren, R., Way, D.A., Moshelion, M., 2015a. Growth and physiological responses of isohydric and anisohydric poplars to drought. EXBOTJ 66, 4373–4381. https://doi.org/10.1093/jxb/erv195.

The control of stomata by water balance - Buckley - 2005 - New Phytologist - Wiley Online Library, (n.d.). ⟨https://nph.onlinelibrary.wiley.com/doi/full/10.1111/j.1469-8137.2005.01543.x⟩ (accessed March 3, 2026).

Farquhar, G.D., Sharkey, T.D., 1982. Stomatal conductance and photosynthesis. Annu. Rev. Plant Biol. 33, 317–345. https://doi.org/10.1146/annurev.pp.33.060182.001533.

Wong, S.C., Cowan, I.R., Farquhar, G.D., 1979. Stomatal conductance correlates with photosynthetic capacity. Nature 282, 424–426. https://doi.org/10.1038/282424a0.

Lawson, T., Kramer, D.M., Raines, C.A., 2012. Improving yield by exploiting mechanisms underlying natural variation of photosynthesis. Curr. Opin. Biotechnol. 23, 215–220. https://doi.org/10.1016/j.copbio.2011.12.012.

Yang, R., Tian, Q., Xu, S., 2006. Mapping quantitative trait loci for longitudinal traits in line crosses. Genetics 173, 2339–2356. https://doi.org/10.1534/genetics.105.054775.

Campbell, M., Momen, M., Walia, H., Morota, G., 2019. Leveraging breeding values obtained from random regression models for genetic inference of longitudinal traits. Plant Genome 12, 180075. https://doi.org/10.3835/plantgenome2018.10.0075.

Moshelion, M., Dietz, K.-J., Dodd, I.C., Muller, B., Lunn, J.E., 2024. Guidelines for designing and interpreting drought experiments in controlled conditions. J. Exp. Bot. 75, 4671–4679. https://doi.org/10.1093/jxb/erae292.

Kerchev, P.I., Van Breusegem, F., 2022. Improving oxidative stress resilience in plants. Plant J. 109, 359–372. https://doi.org/10.1111/tpj.15493.

Sinclair, T.R., 2011. Challenges in breeding for yield increase for drought. Trends Plant Sci. 16, 289–293. https://doi.org/10.1016/j.tplants.2011.02.008.

Snowdon, R.J., Wittkop, B., Chen, T.-W., Stahl, A., 2021. Crop adaptation to climate change as a consequence of long-term breeding. Theor. Appl. Genet 134, 1613–1623. https://doi.org/10.1007/s00122-020-03729-3.

Snow, M.D., Tingey, D.T., 1985. Evaluation of a system for the imposition of plant water stress. Plant Physiol. 77, 602–607. https://doi.org/10.1104/pp.77.3.602.

Negin, B., Moshelion, M., 2016. The advantages of functional phenotyping in pre-field screening for drought-tolerant crops. Funct. Plant Biol. 44, 107–118. https://doi.org/10.1071/FP16156.

Tardieu, F., Simonneau, T., 1998. Variability among species of stomatal control under fluctuating soil water status and evaporative demand: modelling isohydric and anisohydric behaviours. J. Exp. Bot. 49, 419–432. https://doi.org/10.1093/jxb/49.Special_Issue.419.

Attia, Z., Domec, J.-C., Oren, R., Way, D.A., Moshelion, M., 2015b. Growth and physiological responses of isohydric and anisohydric poplars to drought. J. Exp. Bot. 66, 4373–4381. https://doi.org/10.1093/jxb/erv195.

Blum, A., 2009. Effective use of water (EUW) and not water-use efficiency (WUE) is the target of crop yield improvement under drought stress. Field Crops Res. 112, 119–123. https://doi.org/10.1016/j.fcr.2009.03.009.

Passioura, J.B., 2012. Phenotyping for drought tolerance in grain crops: when is it useful to breeders? Funct. Plant Biol. 39, 851–859. https://doi.org/10.1071/FP12079.

Guo, T., Tian, C., Chen, C., Duan, Z., Zhu, Q., Sun, L.Z., 2020. Growth and carbohydrate dynamic of perennial ryegrass seedlings during PEG-simulated drought and subsequent recovery. Plant Physiol. Biochem. 154, 85–93. https://doi.org/10.1016/j.plaphy.2020.06.008.

Chen, D., Wang, S., Cao, B., Cao, D., Leng, G., Li, H., Yin, L., Shan, L., Deng, X., 2016. Genotypic variation in growth and physiological response to drought stress and re-watering reveals the critical role of recovery in drought adaptation in maize seedlings. Front. Plant Sci. 6. https://doi.org/10.3389/fpls.2015.01241.

Sinclair, T.R., 2018. Effective water use required for improving crop growth rather than transpiration efficiency. Front. Plant Sci. 9. https://doi.org/10.3389/fpls.2018.01442.

Lupo, Y., Moshelion, M., 2024. The balance of survival: comparative drought response in wild and domesticated tomatoes. Plant Sci. 339, 111928. https://doi.org/10.1016/j.plantsci.2023.111928.

Ullmann, I., Lange, O.L., Ziegler, H., Ehleringer, J., Schulze, E.-D., Cowan, I.R., 1985. Diurnal courses of leaf conductance and transpiration of mistletoes and their hosts in Central Australia. Oecologia 67, 577–587. https://doi.org/10.1007/BF00790030.

Resco de Dios, V., Loik, M.E., Smith, R., Aspinwall, M.J., Tissue, D.T., 2016. Genetic variation in circadian regulation of nocturnal stomatal conductance enhances carbon assimilation and growth. Plant Cell Environ. 39, 3–11. https://doi.org/10.1111/pce.12598.

Bacher, H., Montagu, A., Herrmann, I., Walia, H., Schwartz, N., Peleg, Z., 2023. Stress-induced deeper rooting introgression enhances wheat yield under terminal drought. J. Exp. Bot. 74, 4862–4874. https://doi.org/10.1093/jxb/erad059.

Teare, I.D., Kanemasu, E.T., 1972. Stomatal-diffusion resistance and water potential of soybean and sorghum leaves. N. Phytol. 71, 805–810. https://doi.org/10.1111/j.1469-8137.1972.tb01959.x.

Hassidim, M., Dakhiya, Y., Turjeman, A., Hussien, D., Shor, E., Anidjar, A., Goldberg, K., Green, R.M., 2017. Circadian clock associated1 (CCA1) and the circadian control of stomatal aperture. Plant Physiol. 175, 1864–1877. https://doi.org/10.1104/pp.17.01214.

Schoppach, R., Sinclair, T.R., Sadok, W., 2020. Sleep tight and wake-up early: nocturnal transpiration traits to increase wheat drought tolerance in a Mediterranean environment. Funct. Plant Biol. 47, 1117. https://doi.org/10.1071/FP20044.

Gosa, S.C., Koch, A., Shenhar, I., Hirschberg, J., Zamir, D., Moshelion, M., 2022b. The potential of dynamic physiological traits in young tomato plants to predict field-yield performance. Plant Sci. 315, 111122. https://doi.org/10.1016/j.plantsci.2021.111122.

Sadok, W., Lopez, J.R., Smith, K.P., 2021. Transpiration increases under high-temperature stress: potential mechanisms, trade-offs and prospects for crop resilience in a warming world. Plant Cell Environ. 44, 2102–2116. https://doi.org/10.1111/pce.13970.

Henry, C., John, G.P., Pan, R., Bartlett, M.K., Fletcher, L.R., Scoffoni, C., Sack, L., 2019. A stomatal safety-efficiency trade-off constrains responses to leaf dehydration. Nat. Commun. 10, 3398. https://doi.org/10.1038/s41467-019-11006-1.

Muir, C.D., Hangarter, R.P., Moyle, L.C., Davis, P.A., 2014. Morphological and anatomical determinants of mesophyll conductance in wild relatives of tomato (olanum sect. ycopersicon, sect. ycopersicoides; Solanaceae). Plant Cell Environ. 37, 1415–1426. https://doi.org/10.1111/pce.12245.

Driscoll, S.P., Prins, A., Olmos, E., Kunert, K.J., Foyer, C.H., 2006. Specification of adaxial and abaxial stomata, epidermal structure and photosynthesis to CO2 enrichment in maize leaves. J. Exp. Bot. 57, 381–390. https://doi.org/10.1093/jxb/erj030.

Lei, Z.Y., Han, J.M., Yi, X.P., Zhang, W.F., Zhang, Y.L., 2018. Coordinated variation between veins and stomata in cotton and its relationship with water-use efficiency under drought stress. Photosynthetica 56, 1326–1335. https://doi.org/10.1007/s11099-018-0847-z.

Zhang, L., Niklas, K.J., Niinemets, Ü., Li, Q., Yu, K., Li, J., Chen, L., Shi, P., 2023. Stomatal area estimation based on stomatal length and width of four Magnoliaceae species: even “kidney”-shaped stomata are not elliptical. Trees 37, 1333–1342. https://doi.org/10.1007/s00468-023-02425-1.

Paradiso, R., de Visser, P.H.B., Arena, C., Marcelis, L.F.M., 2020. Light response of photosynthesis and stomatal conductance of rose leaves in the canopy profile: the effect of lighting on the adaxial and the abaxial sides. Funct. Plant Biol. 47, 639–650. https://doi.org/10.1071/FP19352.

Crawford, J.D., Mayfield-Jones, D., Fried, G.A., Hernandez, N., Leakey, A.D.B., 2025. Stomata in-sight: integrating live confocal microscopy with leaf gas exchange and environmental control. Plant Physiol. 199, kiaf600. https://doi.org/10.1093/plphys/kiaf600.